Approach of a digital twin for the high-frequency dynamics (FMR) of arbitrarily shaped, symmetric ferromagnetic polycrystalline samples

K. Seemann

Karlsruhe Institute of Technology KIT, Institute for Applied Materials, Kaiserstraße 12, 76131 Karlsruhe, Germany

Keywords:
demagnetisation
ferromagnetic anisotropy
FMR
eddy-currents
resonance damping

A B S T R A C T

Soft polycrystalline ferro- or ferrimagnetic materials of arbitrary but symmetrical shape, which form their static magnetisation behaviour according to the demagnetisation Tensor **N**, were theoretically described in terms of their high-frequency dynamics and precession damping of the magnetic moments on the dependence of their microstructure, i.e., the grain size in association with the magneto-crystalline anisotropy. As the basic equation the Landau-Lifschitz-Gilbert (LLG) differential equation was used, in order to establish a general solution which expresses the frequency-dependent magnetisation, magnetic susceptibility $\chi(f)$ and permeability $\mu(f)$ spectra. By means of two examples, films and spherules, we present the dynamics when exposed to a high-frequency wave by taking parameters like the resistivity ρ_m, magneto-crystalline coefficient K_1, uniaxial anisotropy H_u, grain size D_{grain}, thickness t_m, diameter d and eddy-current generation into account. Damping of the magnetic spins is conspicuous by regarding the full width at half maximum (FWHM) of the frequency-dependent imaginary part of the permeability, and in this connection, the effective damping parameter α_{eff} which represents intrinsic as well as extrinsic damping mechanisms. In the papeŕs context, the latter are caused by grains of various size and generate energy dissipating two-magnon scattering.

The goal is to make a first step of an approach for a digital twin which ought to allow the prediction of the dynamic behaviour of ferromagnetic components. They are employed in r.f. devices like cores in (micro) inductors, memory storage devices, etc. or used for basic magnetisation dynamics research. The calculations were conducted by availing the mathematical program MAPLE. Various shapes and parameters now enable to conceive a variety of r.f. components and their very properties.

1. Introduction

Magnetic moments of ferro-ferrimagnetic samples, which are exposed to electromagnetic high-frequency waves, are excited to precess about a direction they are forced to by several types of anisotropies. The well-established Landau-Lifschitz-Gilbert differential equation (LLG) [1] describes the precession and resonance behaviour in an excellent kind of way if the ferromagnetic sample is not too small [2–6]. But more attention must be paid to the sample shape which significantly determines the magnetisation or polarisation and the ferromagnetic frequency behaviour by demagnetisation effects. The dynamics of spin precession also underlies, like each periodically excided system, different damping mechanisms which in summary impact the magnetic spins from being driven away from their energy equilibrium. These mechanisms can be divided, e.g., in intrinsic (spin–orbit exchange, ordinary- and spin flip scattering) and extrinsic (two-magnon scattering) damping mechanisms [7–10]. For technological applications, they can be adequately regarded by a global damping parameter term. It is crucial to consider an additional damping process which originates from eddy-currents [11]. They in turn depend on the resistivity and permeability of the magnetic sample, and they are described and regarded by taking the Maxwell equations into account [12]. A more precise description of the frequency behaviour and ferromagnetic resonance frequency (FMR) can be made by including material constitutions like the grain diameter-dependent mean magneto-crystalline anisotropy [13,14] to the theoretical construct which is able to decisively affect FMR as well as the course of the frequency-dependent permeability.

At this point, the present paper intends to elaborate a digital twin for a body made of ferri- or ferromagnetic material with a certain percentage of a single ferri- or ferromagnetic phase which features a dimensionally symmetric shape. Consequently, geometric considerations allow to derive a sample from an ellipsoid and to express its demagnetisation state by the symmetric demagnetisation tensor. In the following, some dependencies shall be illustrated, in order to show how

E-mail address: klaus.seemann@kit.edu.

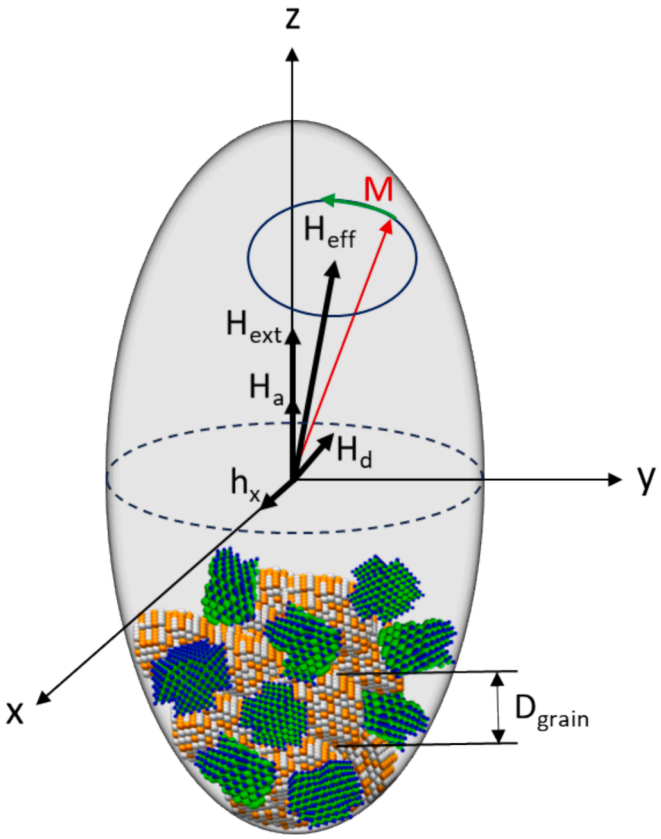

Fig. 1. Ellipsoidal shaped ferromagnetic sample. The field parameters are shown in an ideal and general state. The various magnetic fields $\mathbf{H_{ext}}$, $\mathbf{H_a}$, $\mathbf{H_d}$, and $\mathbf{h_x}$ which generate the effective field, $\mathbf{H_{eff}}$. **M** is the magnetic field vector (magnetic macro spin) which precesses about $\mathbf{H_{eff}}$. The microstructure of a nanocomposite is indicated at the bottom of the ellipsoid. The nonmagnetic grains (crystallites) are illustrated with blue and green and the magnetic phase with white and orange atoms which generates $\mathbf{H_a}$.

the spin dynamics conspicuously differs by two examples of very different shape while varying distinctive material parameters.

2. Theoretical elaboration

2.1. General solution of the basic Landau-Lifschitz-Gilbert (LLG) differential equation

The Landau-Lifschitz-Gilbert differential quasi classical equation

$$\frac{\partial \vec{M}}{\partial t} = \gamma_{eff} \bullet \vec{M} \times \vec{H}_{eff} + \frac{\alpha_{eff}}{M_s} \bullet \left(\vec{M} \times \frac{\partial \vec{M}}{\partial t} \right) \tag{1}$$

is well established as an all-comprehensive tool for the dynamic description of ferromagnetic objects which are exposed to a high-frequency TEM wave. It allows to consider the magnetic system which interacts with the electromagnetic wave as a precessing macro spin about the direction it is forced to by a magnetic anisotropy field and/or an external static magnetic field. Here in its general form, M is the magnetisation, H_{eff} is the effective magnetic field, γ_{eff} is the effective gyromagnetic constant and α_{eff} the effective damping parameter which represents a sum of various damping mechanisms explained in detail elsewhere. The effective magnetic field H_{eff} is the most influential magnitude which, in the following context, deserves a closer view, in order to solve the equation for the universal use in terms of the magnetic sample shape, and in order to feature the frequency-dependent susceptibility or permeability, respectively. A magnetic material generates a demagnetisation field due to its shape which is reverse to a static or alternating high-frequency external field. This demagnetisation field originates from dipole-dipole interaction. Assuming a small ellipsoid as a general sample shape (Fig. 1), sub-shapes can be derived from it which allows to calculate the effective magnetic field inside the considered ferri- or ferromagnet. In the ellipsoid, the microstructure of a poly-crystalline nanocomposite material with nonmagnetic grains (blue and green atoms) and the magnetic phase with the mean grain diameter D_{grain} (white and orange atoms) is also indicated.

A demagnetisation tensor **N**

$$\mathbf{N} = \begin{pmatrix} N_{xx} & 0 & 0 \\ 0 & N_{yy} & 0 \\ 0 & 0 & N_{zz} \end{pmatrix} \tag{2}$$

in combination with the magnetisations m_x, m_y and m_z defines the shape anisotropy field $\mathbf{H_d} = \mathbf{-N \cdot m}$ of the sample which may lower the magnetic field inside the sample according to the various directions. The tensor is symmetric and becomes diagonal if the axes a, b, and c of the ellipsoid coincide with the axes x, y, and z of the coordinate system it is located in. For a uniformly magnetised ellipsoid and its degenerate sub-shapes the trace of the demagnetisation tensor **N** must always be equal to 1. The tensor components N_{xx}, N_{yy} and N_{zz} are calculated by means of the following integrals which represent the demagnetisation factors [15–17]

$$N_{xx} = \frac{a \bullet b \bullet c}{2} \int_0^\infty \frac{1}{(s+a^2) \bullet \sqrt{(s+a^2) \bullet (s+b^2) \bullet (s+c^2)}} ds \tag{3}$$

$$N_{yy} = \frac{a \bullet b \bullet c}{2} \int_0^\infty \frac{1}{(s+b^2) \bullet \sqrt{(s+a^2) \bullet (s+b^2) \bullet (s+c^2)}} ds \tag{4}$$

$$N_{zz} = \frac{a \bullet b \bullet c}{2} \int_0^{\infty} \frac{1}{(s+c^2) \bullet \sqrt{(s+a^2) \bullet (s+b^2) \bullet (s+c^2)}} ds \tag{5}$$

in which a, b and c are now the dimensions of the magnetic sample in the x-, y- and z-direction, respectively. There is no analytical solution for the integrals, so they must be calculated numerically.

We can now formulate the effective magnetic field as follows:

$$\begin{aligned} \vec{H}_{eff} &= \vec{H}_a + \vec{H}_{ext} + \vec{h}_{HF} + \vec{H}_d \\ &= \begin{pmatrix} 0 \\ 0 \\ H_u + H_{cr} \end{pmatrix} + \begin{pmatrix} 0 \\ 0 \\ H_z \end{pmatrix} + \begin{pmatrix} h_x \\ 0 \\ 0 \end{pmatrix} + \begin{pmatrix} N_{xx} & 0 & 0 \\ 0 & N_{yy} & 0 \\ 0 & 0 & N_{zz} \end{pmatrix} \bullet \begin{pmatrix} m_x \\ m_y \\ m_z \end{pmatrix} \\ &= \begin{pmatrix} 0 \\ 0 \\ H_u + H_{cr} \end{pmatrix} + \begin{pmatrix} 0 \\ 0 \\ H_z \end{pmatrix} + \begin{pmatrix} h_x \\ 0 \\ 0 \end{pmatrix} + \begin{pmatrix} N_{xx} \bullet m_x \\ N_{yy} \bullet m_y \\ N_{zz} \bullet m_z \end{pmatrix} \end{aligned} \tag{6}$$

To simplify matters, we assume H_u and an optional anisotropy-increasing external field $\mathbf{H_{ext}}$ in the z-direction. The high-frequency field h_{HF} is assumed to be in the x-direction. H_u is the uniaxial anisotropy field which faces an effective magneto-crystalline anisotropy field H_{cr}. It affects the spin dynamics under certain conditions which is shown in following chapters. As a result, equation (1) changes to the more practical form

$$\begin{pmatrix} \frac{\partial m_x}{\partial t} \\ \frac{\partial m_y}{\partial t} \\ \frac{\partial m_z}{\partial t} \end{pmatrix} = \gamma_{eff} \bullet \begin{pmatrix} m_x \\ m_y \\ m_z \end{pmatrix} \times \begin{pmatrix} h_x & N_{xx} \bullet m_x \\ N_{yy} \bullet m_y \\ H_u + H_{cr} + H_z & N_{zz} \bullet m_z \end{pmatrix} + \frac{\alpha_{eff}}{M_s} \bullet \begin{pmatrix} m_x \\ m_y \\ m_z \end{pmatrix} \times \begin{pmatrix} \frac{\partial m_x}{\partial t} \\ \frac{\partial m_y}{\partial t} \\ \frac{\partial m_z}{\partial t} \end{pmatrix} \tag{7}$$

which turns into a system of first order linear differential equations. As M is close to M_s and $m_z \ll M$, one can assume $\partial m_z/\partial t \approx 0$. After working out (7), we have a system of three differential equations,

$$\frac{\partial m_x}{\partial t} = \gamma_{eff} \bullet \left(m_y \bullet \left(H_u + H_{cr} + H_z \quad M_s \bullet \left(N_{zz} \quad N_{yy} \right) \right) \right) \quad \alpha_{eff} \bullet \frac{\partial m_y}{\partial t} \tag{8}$$

$$\frac{\partial m_y}{\partial t} = \gamma_{eff} \bullet \left(m_x \bullet \left(\left(H_u + H_{cr} + H_z \right) \quad M_s \bullet \left(N_{zz} \quad N_{xx} \right) \right) + M_s \bullet h_x \right) + \alpha_{eff} \bullet \frac{\partial m_x}{\partial t} \tag{9}$$

$$\frac{\partial m_z}{\partial t} \approx 0 \tag{10}$$

at which the I. and II. coupled equations are used to eliminate one derivative in each. Consequently, one must set II into I, and vice versa, in order to obtain two inhomogeneous differential equation for the timed magnetisations m_x and m_y, respectively.

$$\frac{\partial m_x}{\partial t} = \gamma_{eff} \bullet \left(\alpha_{eff} \bullet \frac{H_u + H_{cr} + H_z + M_s \bullet (N_{zz} \quad N_{xx})}{1 + \alpha_{eff}^2} \bullet m_x \quad \frac{H_u + H_{cr} + H_z + M_s \bullet \left(N_{zz} \quad N_{yy} \right)}{1 + \alpha_{eff}^2} \bullet m_y + \alpha_{eff} \bullet \frac{M_s}{1 + \alpha_{eff}^2} \bullet h_x(t) \right) \tag{11}$$

$$\frac{\partial m_y}{\partial t} = \gamma_{eff} \bullet \left(\frac{H_u + H_{cr} + H_z \quad M_s \bullet (N_{zz} \quad N_{xx})}{1 + \alpha_{eff}^2} \bullet m_x \quad \alpha_{eff} \bullet \frac{H_u + H_{cr} + H_z \quad M_s \bullet \left(N_{zz} \quad N_{yy} \right)}{1 + \alpha_{eff}^2} \bullet m_y \quad \frac{M_s}{1 + \alpha_{eff}^2} \bullet h_x(t) \right) \tag{12}$$

The high-frequency field $\mathbf{h_{HF}}$ is assumed to be uniform and considered in the x-direction only. Its wavelength is greater than the dimensions of the ellipsoidal sample, so all approaches made endure. The fact, that we postulate a uniaxial anisotropy, a uniformly magnetised sample, which embodies a single or at least a 180° domain state, and $h_x(t) = h_{x0} e^{i\omega t} << H_u + H_z$, the equations can be linearised and the following assumption can be made: $m_x(\omega)/h_x(\omega) = \chi_{xx}(\omega)$, $m_y(\omega)/h_x(\omega) = \chi_{xy}(\omega)$.

By considering the term $1 + \alpha_{eff}^2 \approx 1$ at this point, and by using the solutions $m_x(t) = m_{x0} e^{i\omega t}$ and $m_y(t) = m_{y0} e^{i\omega t}$ with their first derivatives $\partial m_x(t)/\partial t = i \cdot \omega \cdot m_{x0} e^{i\omega t}$ and $\partial m_y(t)/\partial t = i \cdot \omega \cdot m_{y0} e^{i\omega t}$, the frequency-dependent susceptibilities end up in the general form

$$\chi_{xx}(\omega) = \frac{\gamma_{eff}^2 \bullet M_s \bullet \left(H_u + H_{cr} + H_z \quad M_s \bullet \left(N_{zz} \quad N_{yy} \right) \right) + i \bullet \omega \bullet \alpha_{eff} \bullet \gamma_{eff} \bullet M_s}{\gamma_{eff}^2 \bullet \left(\left(H_u + H_{cr} + H_z + M_s \bullet (N_{xx} \quad N_{zz}) \right) \bullet \left(H_u + H_{cr} + H_z \quad M_s \bullet (N_{zz} \quad N_{yy}) \right) \right) + i \bullet \omega \bullet \gamma_{eff} \bullet \alpha_{eff} \bullet \left(2 \bullet \left(H_u + H_{cr} + H_z \right) + M_s \bullet (N_{yy} \quad N_{xx}) \right) \quad \omega^2} \tag{13}$$

$$\chi_{xy}(\omega) = \frac{i \bullet \omega \bullet \gamma_{eff} \bullet M_s}{\gamma_{eff}^2 \bullet \left(\left(H_u + H_{cr} + H_z + M_s \bullet (N_{xx} \quad N_{zz}) \right) \bullet \left(H_u + H_{cr} + H_z \quad M_s \bullet (N_{zz} \quad N_{yy}) \right) \right) + i \bullet \omega \bullet \gamma_{eff} \bullet \alpha_{eff} \bullet \left(2 \bullet \left(H_u + H_{cr} + H_z \right) + M_s \bullet (N_{yy} \quad N_{xx}) \right) \quad \omega^2} \tag{14}$$

The ferromagnetic resonance frequency can be calculated from the homogeneous parts of the differential equations (11) and (12). It results in a precise expression according to [4]

$$f_{FMR} = \frac{\gamma_{eff} \bullet \mu_0}{2 \bullet \pi \bullet \left(1 + \alpha_{eff}^2\right)} \bullet \sqrt{(H_u + H_{cr} + H_z)^2 + (H_u + H_{cr} + H_z) \bullet M_s \bullet \left(N_x + N_y \quad 2N_z\right) + M_s^2 \bullet (N_z \quad N_x) \bullet \left(N_z \quad N_y\right) \quad \alpha_{eff}^2 \bullet \frac{M_s^2 \bullet \left(N_x \quad N_y\right)^2}{4}} \tag{15}$$

at which the damping parameter makes an impact.

2.2. The advanced solution of the Landau-Lifschitz-Gilbert differential equation

Up to now, eddy-currents were neglected which in turn depend on the permeability μ(f) and on the material resistivity ρ_m. We now use the equations (13) and (14) to form the frequency-dependent permeability by introducing $\omega = 2 \cdot \pi \cdot f$ and the Maxwell high-frequency field distribution due to eddy-current generation [3,12]

$$h_x(f,y) = h_{x0} \bullet e^{i \bullet 2 \bullet \pi \bullet f \bullet t} \bullet \frac{e^{i \bullet \lambda_m \bullet y} + e^{-i \bullet \lambda_m \bullet y}}{e^{i \bullet \lambda_m \bullet \frac{t_m}{2}} + e^{-i \bullet \lambda_m \bullet \frac{t_m}{2}}} \tag{16}$$

The high-frequency field $h_x(f,y)$ changes in the y-direction according to the ellipsoid extension parameter b and is her interpreted as the magnetic material thickness t_m in case of a film or the diameter d of a spherule (bulk material). λ_m is a complex formula delineated by

$$\lambda_m = (1 \quad i) \bullet \sqrt{\frac{2 \bullet \pi \bullet f \bullet \mu_0 \bullet (1 + \chi_x(f))}{2 \bullet \rho_m}} = (1 \quad i) \bullet \frac{1}{\delta_{skin}(f)} \tag{17}$$

It represents the wave number of $h_x(f,y)$ which penetrates the material with the skin depth $\delta_{skin}(f)$.

In order to obtain the high-frequency field distribution in the sample, equation (16) must be integrated over its dimension, i.e., its thickness t_m or a diameter d.

By means of all these equations it is possible to establish the nearly all-encompassing formulas of the frequency-dependent permeability

$$\mu_{xx}(f) = \frac{m_x(f)}{h_x(f,y)} + 1 = \frac{m_{x0} \bullet e^{i \bullet 2 \bullet \pi \bullet f \bullet t}}{h_{x0} \bullet e^{i \bullet 2 \bullet \pi \bullet f \bullet t} \bullet \frac{1}{2 \bullet t_m} \bullet \int_{\frac{-t_m}{2}}^{\frac{t_m}{2}} \frac{e^{i \bullet \lambda_m \bullet y} + e^{i \bullet \lambda_m \bullet y}}{e^{i \bullet \lambda_m \bullet \frac{t_m}{2}} + e^{i \bullet \lambda_m \bullet \frac{t_m}{2}}} dy} + 1 =$$

$$= \chi_{xx}(f) \bullet \frac{2 \bullet \left(e^{i \bullet \lambda_m \bullet \frac{t_m}{2}} \quad e^{-i \bullet \lambda_m \bullet \frac{t_m}{2}}\right)}{i \bullet \lambda_m \bullet t_m \bullet \left(e^{i \bullet \lambda_m \bullet \frac{t_m}{2}} + e^{-i \bullet \lambda_m \bullet \frac{t_m}{2}}\right)} + 1 \tag{18}$$

$$\mu_{xy}(f) = \chi_{xy}(f) \bullet \frac{2 \bullet \left(e^{i \bullet \lambda_m \bullet \frac{t_m}{2}} \quad e^{-i \bullet \lambda_m \bullet \frac{t_m}{2}}\right)}{i \bullet \lambda_m \bullet t_m \bullet \left(e^{i \bullet \lambda_m \bullet \frac{t_m}{2} \bullet} + e^{-i \bullet \lambda_m \bullet \frac{t_m}{2}}\right)} \tag{19}$$

As soft ferromagnetic materials are usually in a fine polycrystalline state, they can still possess a mean magneto-crystalline anisotropy $< K_{1mean} >$ coefficient dependent on the grain diameter D_{grain} [14] which perturbs the precession of the magnetic moments. This may cause higher damping, i.e., higher broadening of the resonance spectrum but also a slight shift of the resonance maximum due to the additional mean magneto-crystalline anisotropy field H_{cr}. One can now frame the afore introduced general anisotropy field as

$$\mu_0 \bullet H_a = \mu_0 \bullet (H_u + H_z) + \mu_0 \bullet H_{cr} = \mu_0 \bullet (H_u + H_z) + \frac{1}{2} \bullet \frac{< K_{1mean} >}{M_s} =$$

$$= \mu_0 \bullet (H_u + H_z) + \frac{1}{2 \bullet M_s} \bullet |K_1| \bullet V_{ph}^2 \bullet \left(\frac{D_{grain}}{l_{ex}}\right)^{\beta} \tag{20}$$

It is well known that as the mean magneto-crystalline anisotropy field H_{cr} in association with D_{grain} causes additional damping. Hence, the effective damping parameter can be defined by $\alpha_{eff} = \alpha_0 + \alpha_{cr}$. With the general approximative relation for line broadening $(\Delta H_{FMR})_{cr}$ in a magnetic domain FMR measurement due to a polycrystalline non-textured structure which assumes small independent, non-interacting grains from [18] and with $\Delta H = 2 \cdot \alpha \cdot \omega_{res} / \gamma$ by a first order approximation [19], the following approach with introducing the mean grain size-dependent moderate crystalline anisotropy, and by neglecting a possible material porosity, was established

$$\Delta H_{FMR} \cong \Delta H_0 + \frac{2 \bullet < K_{1mean} >}{M_s} = \frac{2 \bullet \alpha_0 \bullet \omega_0}{\gamma_{eff}} + \frac{2 \bullet < K_{1mean} >}{M_s}$$

$$= \frac{2 \bullet \alpha_{eff} \bullet \omega_{FMR}}{\gamma_{eff}} \tag{21}$$

With the aid of [14] and with $\omega_{res} \quad \omega_0 \approx \omega_{FMR}$ due to moderate mean crystalline anisotropies the expression for the effective damping parameter can be approximated for a material with one ferri- or ferromagnetic phase,

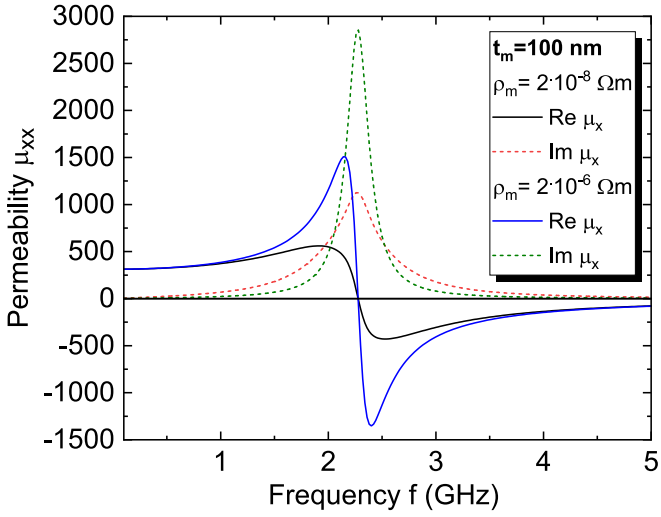

Fig. 2. Real- and imaginary part of the frequency-dependent permeability of a 100 nm thick ferromagnetic film for two different resistivities. The ferromagnetic resonance frequency amounts to 2.26 GHz. An intrinsic damping parameter of α_0 0.006 was used for computation. A grain diameter of 2 nm was assumed for calculation.

$$\alpha_{eff} = \alpha_0 + \frac{\gamma_{eff} \bullet |K_1| \bullet V_{ph}^2 \bullet \left(\frac{D_{grain}}{l_{ex}}\right)^{\beta}}{2 \bullet \pi \bullet f_{FMR} \bullet M_s} \tag{22}$$

in which α_0 is assumed as the damping parameter that shall represent intrinsic damping effects. ω_0 would be the ferromagnetic resonance frequency for an ideal material without extrinsic damping. The exponent β ideally set to 6 for a single magnetic phase material but can also be 3 in a certain range due to additional phases and/or magnetoelastic effects and even induced anisotropies. $|K_1|$ is the absolute value of the nominal crystalline anisotropy coefficient, V_{ph} the ferromagnetic material phase volume fraction and l_{ex} the exchange length. All assumptions made endure for $D_{grain} < l_{ex}$ for which a fair soft ferromagnetic state can be expected. In order to keep the theoretical concept coherent, a cubic crystal structure slips in the calculations, and to keep track of things, we assume an independent grain approximation for grains in a nonmagnetic matrix, so we neglect possible "dipole narrowing" between the grains. The last term represents the aspect of extrinsic damping at which two-magnon activities take place through perturbing the uniform precession by various grain orientations.

3. Discussion of frequency-dependent permeability spectra by parameter studies for different sample shapes

The following chapter shall examine the permeability spectra how they behave on relevant parameters. The focus will be put on the material resistivity ρ_m and the sample dimensions, respectively, as well as the impact of the $< K_{1mean} >$ which may sensitively change with the grain diameter. For most calculations, we neglect a static external field H_z. The samples are considered as being uniformly magnetised due to the uniaxial anisotropy H_u itself, so that the magnetic moments perform a uniform precession mode. Perturbations, which are caused, e.g., by possible intrinsic damping mechanisms like spin flip, ordinary scattering of magnetic electrons with the lattice or three- and four-magnon scattering are implicitly assumed by the overall damping parameter α_0.

3.1. *Variation of the material resistivity and thickness of film samples*

The basic parameters arbitrarily used for computation possess the following values: $\gamma_{eff} = 180$ GHz/T, $\alpha_0 = 0.006$, $\mu_0 H_u = 0.0045$ T, $H_z = 0$, $\mu_0 M_s = 1.4$ T, $K_1 = 30000$ J/m^3. As we consider thin films with the thickness assumed along the y-direction and much lower than its lateral dimensions, the demagnetisation factors approximatively calculate to $N_{xx} = 0$, $N_{yy} = 1$ and $N_{zz} = 0$. Then, formula (15) results in

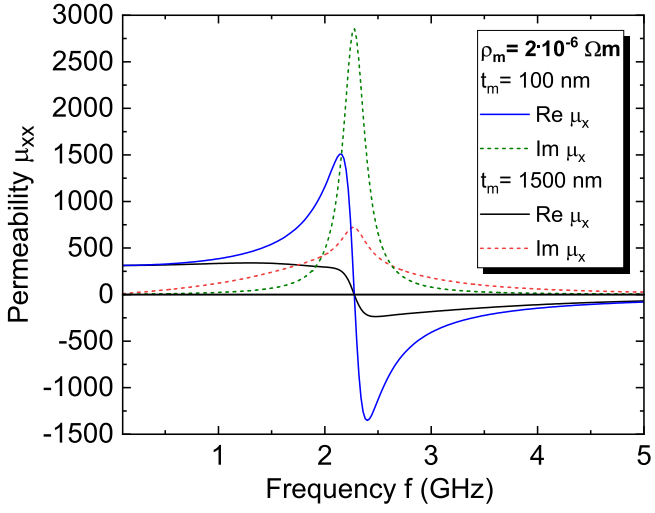

Fig. 3. Real- and imaginary part of the frequency-dependent permeability of a 100 nm and 1500 nm thick ferromagnetic film with a resistivity of ρ_m $2{\cdot}10^{-6}$ Ωm, respectively. FMR amounts to around 2.26 GHz. An intrinsic damping parameter of α_0 0.006 was used for computation. A grain diameter of 2 nm was assumed for calculation.

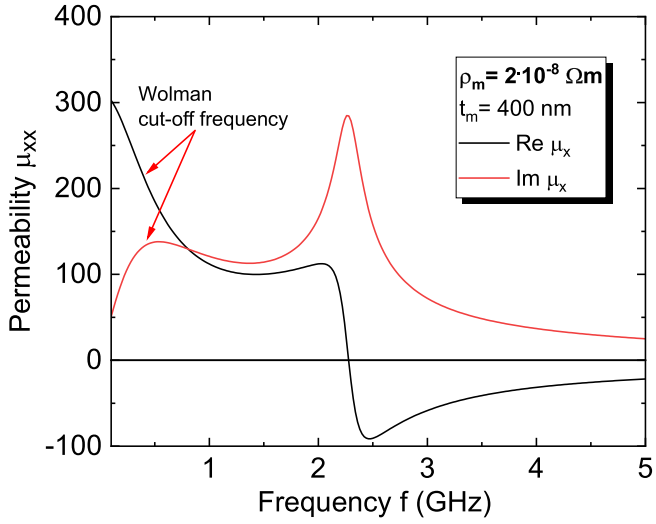

Fig. 4. Real- and imaginary part of the frequency-dependent permeability of a 400 nm and thick ferromagnetic film with a low resistivity of ρ_m $2{\cdot}10^{-8}$ Ωm. The Wolman cut-off frequency amounts to around 400 MHz indicated by the red arrows. An intrinsic damping parameter of α_0 0.006 was used for computation. A grain diameter of 2 nm was assumed for calculation.

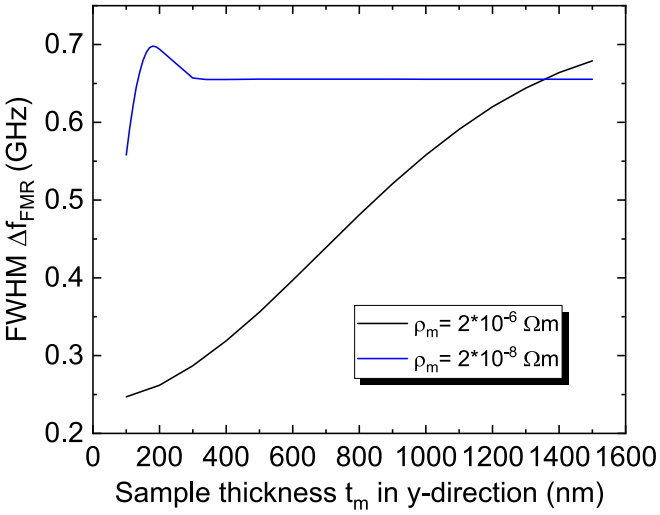

Fig. 5. Full width at half maximum (FWHM) of the imaginary part of the complex permeability dependent on the sample thickness for two different resistivities. An intrinsic damping parameter of α_0 0.006 was used for computation. A grain diameter of 2 nm was assumed for calculation.

$$f_{FMR} = \frac{\gamma_{eff} \bullet \mu_0}{2 \bullet \pi \bullet \left(1 + \alpha_{eff}^2\right)} \bullet \sqrt{(H_u + H_{cr} + H_z)^2 + (H_u + H_{cr} + H_z) \bullet M_s + \alpha_{eff}^2 \bullet \frac{M_s^2}{4}} \tag{23}$$

The lower the resistivity the less the penetration depth of the high-frequency field into a ferromagnetic sample which excites the ferromagnetic moments to precess about the effective field which is predominantly determined by the uniaxial field. In Fig. 2, it can be observed how the resistivity impacts the shape of the real and imaginary part of the spectra for a, e.g., 100 nm thick film. For calculation, the grain

diameter D_{grain} is kept for the time being at 2 nm in diameter, so that the mean magneto-crystalline anisotropy coefficient does not impact the spectra. If the resistivity is low eddy-currents can arise much easier than for materials with higher resistivity. High eddy-current generation causes an induced magnetic eddy-current field which interferes with the external high-frequency field. Consequently, the external high-frequency field is attenuated, or shielded and cannot totally interact with the magnetic moments. On the other hand, there is a phase shift between the exiting and the shielding eddy-current field which inhibits the exiting spin-driving high-frequency field.

As a result, additional loss of the precessing magnetic spin system occurs which is reflected by additional broadening of the frequency spectra. This does not contribute or is considered as a part of the damping parameter because it is directly caused by the interaction of external and induced magnetic fields.

Basically, eddy-currents influence the penetration depth of the external high-frequency field which is described by the skin depth. As formulated in (17) the equation is determined by the frequency, permeability and resistivity. By increasing the film material thickness, only the high-frequency field-pervaded part of the sample, according to the skin depth, excides the magnetic moments to precess. The remaining spins, which are not distinctly exposed to the high-frequency field, function as a spin brake or spin sink. This can be considered as a perturbation which leads to consequent damping of the actively excited moments and is shown by means of the two spectra in Fig. 3. For this calculation, the film material thickness was increased from 100 to 1500 nm. For appropriate resistivities and in a wide range of thickness, the permeability spectra are clearly characterised by their ferromagnetic resonance frequency at which the energy of the external high-frequency field is absorbed by the spin system and dissipated according to the strength of damping. If the resistivity is critically low the precession of the magnetic moments already sustains a strong impact at a low material thickness due to the immense dispersion of eddy-currents. It results in a sudden decrease of the permeability defined by the Wolman cut-off frequency at which the real part of the permeability declines to 2/3 of the initial real part $\mu_x(f \rightarrow 0)$. It can be estimated by the equation,

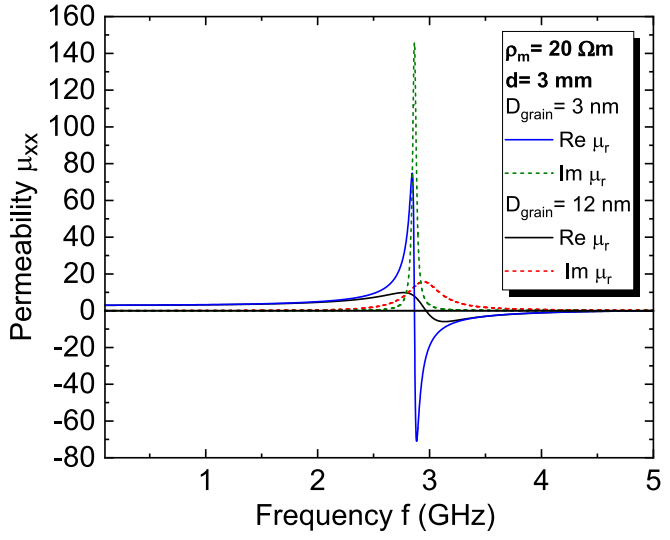

Fig. 6. Real- and imaginary part of the frequency-dependent permeability of two ferromagnetic spherules with different grain sizes and a diameter of 3 mm, respectively. A magneto-crystalline anisotropy coefficient of 10000 J/m^3 was applied in the calculation. The parameter d plays now role of a "thickness" and represents b according to the y-direction of the ellipsoid. An intrinsic damping parameter of α_0 0.006 was used for computation. The effective damping α_{eff} $\alpha_0 + \alpha_{cr}$ results from the calculation.

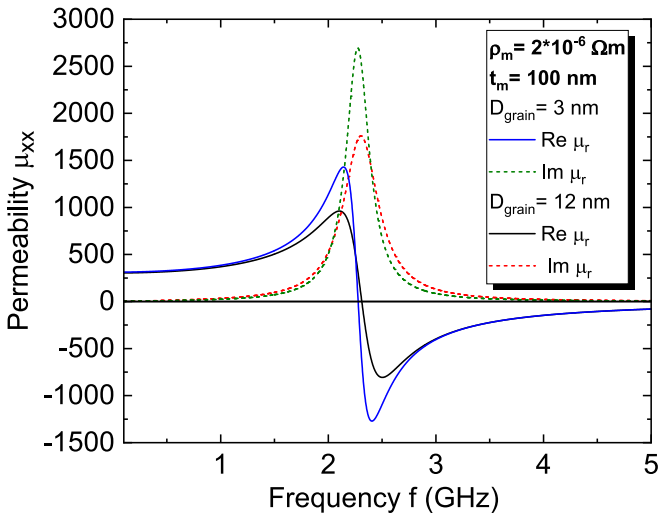

Fig. 7. Real- and imaginary part of the frequency-dependent permeability of two ferromagnetic films with different grain sizes, respectively. A magneto-crystalline anisotropy coefficient of 10000 J/m^3 was applied in the calculation. An intrinsic damping parameter of α_0 0.006 was used for computation. The effective damping α_{eff} $\alpha_0 + \alpha_{cr}$ results from the calculation.

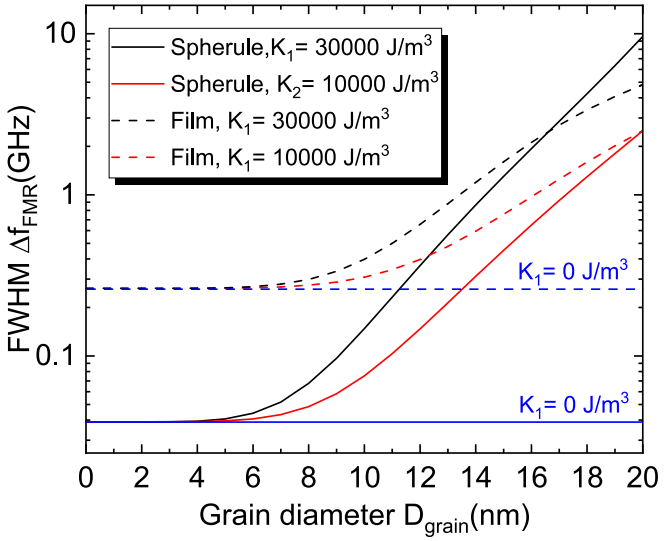

Fig. 8. Full width at half maximum (FWHM) of resonance spectra on the dependence of the grain diameter for different magneto-crystalline anisotropy coefficients K_1. The dependencies are calculated for spherule- and film-shaped samples. The damping parameter α_0 amounts to 0.006, β 6.

$$f_{wc} = \frac{4 \bullet \rho_m}{\pi \bullet \mu_0 \bullet \left(\frac{J_s}{\mu_0 \bullet H_a} + 1\right) \bullet t_m^2} \tag{24}$$

As one can easily observe for an extreme case (Fig. 4), the Wolman cut-off frequency is much lower than the FMR of 2.26 GHz. By means of equation (24) the cut-off frequency calculates to around 400 MHz which is indicated by the red arrows.

Here, the imaginary part of permeability shows a first broad maximum which agrees with an eddy-current driven energy dissipation. As one can see in the Figs. 2 to 4, the system of precessing spins is quite sensitive to the variation of the resistivity, and accordingly, to the material thickness. This is illustrated in Fig. 5, in which the full width at half maximum Δf_{FMR} (FWHM) of the imaginary part of the spectra is plotted against the sample thickness for two different resistivities. As the skin

depth clearly drops with the square root it is the initial and predominant origin for the immense increase of the FWHM versus the material thickness, just for low resistivities. For a higher resistivity, a moderate rise of the FWHM can be denoted due to a somewhat more inhibited eddy-current evolution. Both plots tend to saturate by virtue of the 1/e drop of the eddy-current density $I = I_0 e^{(f)/\delta}$, where they do not noticeably change for higher frequencies after it has caused "Wolman losses".

3.2. Variation of the material grain size in a spherule and a thin film

To demonstrate the impact of the grain size, a sample dimension is chosen which represents bulk material. In FMR experiments, spherules are frequently used due to their symmetry which generates the demagnetisation factors $N_{xx} = N_{yy} = N_{zz} = 1/3$. It reduces equation (15) to the simple expression

$$f_{FMR} = \frac{\gamma_{eff} \bullet \mu_0}{2 \bullet \pi \bullet \left(1 + \alpha_{eff}^2\right)} \bullet (H_u + H_{cr} + H_z) \tag{25}$$

As one can easily recognise the ferromagnetic resonance frequency is not influenced by the saturation magnetisation anymore. But for computation of the spectra a magnetisation of $\mu_0 M_s = 0.02$ T and an external field of $\mu_0 H_z = 0.1$ T was applied, in order to assume a magnetically saturated sample which cannot be featured by the uniaxial one. Hence, for such a high external field, the uniaxial anisotropy as previously defined would not play a role anymore because it appears weak in comparison to H_z but shifts FMR to frequencies obtained in films to make the frequency behaviour more comparable. As it is about a bulk sample the resistivity should be sufficiently high, so eddy-currents are less effective. This results in a high skin depth which enables the entire spin ensemble to precess about the anisotropy field, i.e., the external field H_z. Now, the influence of the mean magneto-crystalline anisotropy, which depends on the grain size, should clearly affect the frequency behaviour, i.e., damping of the dynamic ferromagnetic system. In Fig. 6, the spectra exhibit that there is a noticeable impact on the damping behaviour of the magnetic spins.

The graph shows the enormous broadening of the spectrum within a grain size increase from 3 to 12 nm. At this point, it is obvious that a mean grain diameter in association with a magneto-crystalline anisotropy causes damping of the magnetic moments, more than any other damping process. This arises from relation (22) in which the grain diameter here continues with the 6th power, like the mean magneto-crystalline anisotropy coefficient $< K_{1mean} >$ in equation (20) does. It can similarly be observed that f_{FMR} increases with the effective mean magneto-crystalline anisotropy field H_{cr} which depends on the mean crystalline anisotropy coefficient $< K_{1mean} >$ and which in turn depends on the nominal crystalline anisotropy coefficient $|K_1|$ consistent with the grain diameter D_{grain}. The increase of the resonance frequency and FWHM due to grain growth also applies to thin films, if sufficiently thick enough, as observed in Fig. 7, but by the way of comparison, films do not seem to show this intense rise of damping.

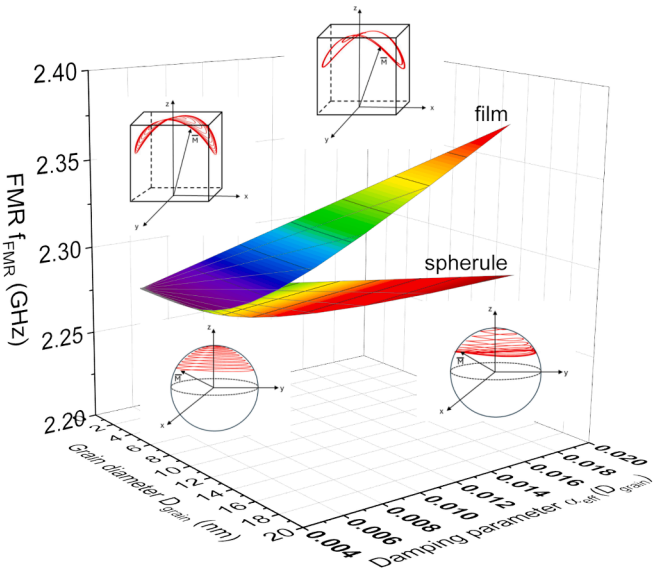

Fig. 9. Ferromagnetic resonance frequency dependent on the grain diameter and the effective damping parameter. The effective damping parameter is dependent on the grain diameter as well. The insets show the calculated trajectories of the precessing magnetic spins at resonance for films and spherules with the grain diameters of 3 nm (left hand side) and 19 nm (right hand side). An intrinsic damping parameter of α_0 0.006 was used for computation. The effective damping α_{eff} $\alpha_0 + \alpha_{cr}$ results from the calculation.

This can be confirmed by Fig. 8 which shows the log-plot of the FWHM for spherules and films, dependent on the grain diameter for two different magneto-crystalline anisotropy coefficients. In contrary to the spherules the FWHMs of the films begin to saturate at a grain diameter of about 16 to 18 nm. The slope of the curves is much lower for the films which reflects the damping behaviour in Figs. 6 and 7. By means of [20] shown for the frequency and [21] in the field domain measurement it can be qualitatively compared that the FWHM increases according to the calculations. In Ref. [22], also conducted in the field domain measurement at distinct frequencies, the FWHM shows this behaviour for films in a comparable way. Here, its saturation is clearly emphasised which generally depends on the magneto crystalline anisotropy coefficient. The fact that the grains are differently oriented, and in this connection is the magneto-crystalline anisotropy, it disturbs the much weaker uniaxial anisotropy which commonly enables a nearly uniform and moderately unperturbed spin precession. By considering the demagnetisation coefficients of a ferromagnetic film the demagnetisation factor in the y-direction is almost equal to 1. As a result, an in-plane uniaxial anisotropy is slightly more supported despite the counteractive magneto-crystalline one. Consequently, in both cases the design of ferromagnetic materials with low frequency losses, i.e., low energy dissipation, requires grains to be as small as possible like in nanocomposites in which a grain reducer impedes diffusion for ferromagnetic grain growth. These grain reducers should be stoichiometric HfN [23] or ZrN which supports the formation of the uniaxial anisotropy. Even by adjusting an appropriate stoichiometry of ferromagnetic element combinations, e.g., Fe-Co can lead to a neglectable magneto-crystalline anisotropy coefficient to keep the grain effect low.

In a next step, the different ferromagnetic transition elements can alternately arrange themselves in a chain-like short-range order within the ferromagnetic microstructure and form the already mentioned uniaxial anisotropy, also called diffusion anisotropy [24], which is triggered by annealing the ferromagnetic material in a static saturation field [25]. In general, a uniaxial anisotropy can also be simultaneously generated and/or increased by an external magnetic field which tilts the magnetic moments according to its direction. If the magneto-crystalline anisotropy is minimised in a way that it can be neglected and if material defects are not considered, the FWHM is basically influenced by the sorts of damping features which are enunciated by the damping parameter α_0.

3.3. FMR frequency behaviour on the dependence of the grain diameter and grain diameter-dependent effective damping parameter

Now we put the focus on the ferromagnetic resonance frequency in relation to the grain diameter D_{grain} which allows to underline the correlation between the microstructure and damping term. Again, we assume the excitation high frequency field in the x-direction. By using formulas (22), (23) and (25) the following Fig. 9 exhibits the FMR frequency behaviour of a thin ferromagnetic film and a spherule dependent on the material grain diameter features. As mentioned above that $\omega_0 = 2 \cdot \pi \cdot f_0 \approx 2 \cdot \pi \cdot f_{FMR}$ in the small grain diameter regime f_{FMR} in equation (22) is considered as an initial FMR frequency. This can be used as an

approach as the FMR frequency changes in a small range and makes the calculation more convenient. For the calculation of the spin trajectories, $5{\cdot}10^{-9}$ s duration of precession time, $K_1 = 10000$ J/m^3 and $\alpha_0 = 0.006$ was utilised. In order to compare the two shapes of a ferromagnetic material, all parameters were chosen in a way that the FMR frequency is on an equal level. It can be clearly observed that the FMR frequency of a spherule is less influenced by the damping parameter and grain diameter, i.e., the concomitant and increasing magneto-crystalline anisotropy, than of a thin film. If one calculates (15) for the individual shapes, one can perceive that the FMR frequency of a spherule does not depend on the saturation magnetisation but on the damping parameter in the first term of (25) only, and linearly on H_{cr} which is quite different to a film. Here, it can be seen that α_{eff} and $H_{cr}(<K_{1mean}>)$ mutually compensate the FMR frequency increase to a certain degree. The fact that the effective damping α_0 and damping due to $< K_{1mean} >$ in association with D_{grain} and in combination with M_s plus $H_{cr}(<K_{1mean}>)$ in combination with M_s is present for a film, the increase of the FMR frequency is obvious (see (23)). The insets of Fig. 9 provide the computed precession behaviour, i.e., the magnetic moment trajectories according to the two sample shapes at the FMR frequency. It is observable that the spin precessions are strikingly influenced by the demagnetisation factors and the damping parameters. Concerning the film system, the precession amplitude of the magnetic moment is strongly inhibited by N_{yy} whereupon the spin in the spherules describes a less unperturbed trace. This is obvious due to the symmetrical conditions at which all demagnetisation factors are equal to 1/3. On the other hand, this also affects the permeability spectra which were introduced in the previous chapters.

4. Conclusion

A more detailed and theoretical elaboration of the dynamic behaviour and the ferromagnetic resonance frequency of ferromagnetic samples of different shapes was conducted by solving the general Landau-Lifschitz-Gilbert differential equation (LLG) in an analytical and computational way. Eddy-currents due to the high-frequency wave impact the samples are subjected, were considered by incorporating the Maxwell equation, so that a modified an all comprising LLG could be established which rounds the description of ferromagnetic resonance phenomena off. Out of it, the equation could be configured in a way to compute every sample shape for which the magnetisation is characterised by the symmetric demagnetisation tensor components. Sample shapes, e.g., thin films and spherules, which visibly represent different magnetic objects, were regarded to demonstrate various features, i.e. damping (α_{eff}, FWHM) and FMR behaviour dependent on the material thickness, resistivity and mean magneto-crystalline anisotropy in accordance with the grain size. Additionally, the theoretical considerations made apply if the magnetic samples possess a nearly uniform magnetisation, i.e., their magnetic domains are uniformly aligned with respect to the external high-frequency field and are moderately perturbed by the magneto crystalline anisotropy only. Especially, films can vary in their characteristics dependent on the thickness and resistivity. Consequently, the resistivity should be high, or the film thickness should be low enough to obtain a permeability spectrum with low precession damping. By comparing ferromagnetic films and spherules of an equal material system the two shapes bear distinctive features. The calculations demonstrate that the increase of the grain diameter generates more impact on the FWHM (linewidth), and similar on the effective damping parameter, for existing magneto-crystalline anisotropies in spherules than the same magneto-crystalline anisotropies in films. On the other hand, the FMR frequency is less affected for spherules, i.e., the increase of the FMR frequency is less enhanced than in thin films, and their spins describe a more steady and unperturbed precession trajectory. The linewidth for spherules comparably commences at much lower values but gradually increase with higher slopes and even outrange the films for grain diameters from around 16 to 18 nm on. Considering the intensities at resonance (e.g. imaginary part of the permeability) the films clearly play a superior role. They exhibit higher intensities by a factor of about 20 in comparison to the spherules. This can obviously be explained by their demagnetisation factor of 1/3 which weakens the high-frequency field and lowers the magnetic spin deflection.

Dependent on the application in high-frequency devices the dynamic characteristics and features of ferro-/ferrimagnetic objects can herewith elaborately calculated, and in this connection, optimised according to the material specifications, constitutions and even to their shapes. So, an approach of a digital twin could be established which allows to design a variety of magnetic r.f. components and their applications. They usually demand low losses, i.e., the permeability shall be kept constant on a certain level as far as possible till the FMR frequency leads to its breakdown.

CRediT authorship contribution statement

K. Seemann: Writing – review & editing, Writing – original draft, Visualization, Validation, Supervision, Software, Methodology, Investigation, Formal analysis, Data curation, Conceptualization.

Declaration of competing interest

The authors declare that they have no known competing financial interests or personal relationships that could have appeared to influence the work reported in this paper.

Data availability

No data was used for the research described in the article.

References

[1] T.L. Gilbert, A phenomenological theory of damping in ferromagnetic materials, IEEE Trans Magn. 40 (2004) 3443.
[2] Y. Nakatani, Y. Uesaka, N. Hayashi, Direct solution of the Landau-Lifschitz-Gilbert equation for micromagnetics, *Jpn. J. Appl. Phys.* 28 (1989) 2485.
[3] K. Seemann, H. Leiste, K. Krüger, Theoretic 3-D study of the high-frequency magnetic moment dynamics in thin ferromagnetic films with in–plane uniaxial anisotropy by considering eddy-current generation, *J. Magn. Magn. Mater.* 324 (2012) 1926.
[4] K. Seemann, H. Leiste, K. Krüger, Alternative theoretical approach of the exact ferromagnetic resonance frequency for common sample shapes by considering the phenomenological damping parameter - a tribute to C. Kittel and T. L. Gilbert, *Magn. Res. Sol., Electronic Journal.* 2014, **16**, 3, 14301.
[5] S.V. Shcherbinin, R. Pérez, M. Vazquez, G.V. Kurlyandskaya, Ferromagnetic resonance in electroplated CuBe, FeCoNi and amorphous CoFeSiB Wires, *IEEE Trans Magn.*, 56 (4) (2020) 2800110.
[6] V.A. Fel'k, S.V. Komogortsev, Ferromagnetic resonance in a microtube, *J. Appl. Phys.* 129 (2021) 183904.
[7] V. Kamberský, On the Landau-Lifschitz relaxation in ferromagnetic metals, *Can. J. Phys.* 48 (1970) 2906.
[8] I. Garate, A. MacDonald, Gilbert damping in conducting ferromagnets. II. model tests of the torque-correlated formula, *Phys. Rev. B* 79 (2009) 064404.
[9] M.J. Hurben, C.E. Patton, Theory of two magnon scattering microwave relaxation and ferromagnetic resonance linewidth in magnetic thin films, *J. Appl. Phys.* 83 (8) (1998) 4344.
[10] B.K. Kuanr, R.E. Camley, Z. Celinski, Extrinsic contribution to Gilbert damping in sputtered NiFe films by ferromagnetic resonance, *J. Magn. Magn. Mater.* 286 (2005) 276.
[11] K. Seemann, H. Leiste, V. Bekker, Uniaxial anisotropy and high frequency permeability of novel soft magnetic FeCoTaN and FeCoAlN films field-annealed at CMOS temperatures, *J. Magn. Magn. Mater.* 283 (2004) 310.
[12] K. Seemann, H. Leiste, V. Bekker, New theoretical approach to the r.f.– dynamics of soft magnetic FeTaN films for CMOS components, *J. Magn. Magn. Mater.* 278 (2004) 200.
[13] G. Herzer, Grain size dependence of coercivity and permeability in nanocrystalline ferromagnets, *IEEE Trans Magn.*, 26 (5) (1990) 1397.
[14] G. Herzer, Anisotropies in soft magnetic nanocrystalline alloys, *J. Magn. Magn. Mater.* 294 (2005) 99.
[15] L. Daniel, R. Corcolle, A note on the effective magnetic permeability of polycrystals, *IEEE TransMagn.*, 43 (7) (2007) 3153.
[16] F. Martin, U. Aydin, D. Singh, L. Daniel, P. Rasilo, A. Belahcen, Demagnetization Field in a Uniformly Magnetized Ellipsoid Embedded in an Infinite Anisotropic Media 1 (2016).
[17] G. Di Fratta, The Newtonian potential and the demagnetizing factors of the general ellipsoid, 2016 *Proc. R. Soc.* **A472**: 20160197.

[18] A.G. Gurevich, G.A. Melkov, Magnetization oscillations and waves, 1996 *CRC Press, Inc.*

[19] S. Krupica, Physik der Ferrite und verwandten magnetischen oxide, 1973 Friedr. Vieweg + Sohn, Braunschweig.

[20] K. Seemann, H. Leiste, A. Kovàcs, Damping and ferromagnetic resonance linewidth broadening in nanocrystalline soft ferromagnetic Fe-Co-Hf-N films, *J. Magn. Magn. Mater.* 320 (2008) 1952.

[21] S. V. Komogortseva, R. S. Iskhakova, P. A. Kuznetsovc, A. I. Belyaevac , G. N. Bondarenkod, and L. A. Chekanovaa, Properties of Ferromagnetic Resonance in Fe73.5CuNb3Si13.5B9 Nanocrystalline Alloys, 2010 *Physics of the Solid State,* **52**, 11. 2287.

[22] R. D. McMichael, A mean-field model of extrinsic line broadening in ferromagnetic resonance, 2008 *J. Appl. Phys.* **103**, 07B114.

[23] K. Seemann, H. Leiste, C. Klever, On the relation between the effective ferromagnetic resonance linewidth Δfeff and damping parameter αeff in ferromagnetic Fe-Co-Hf-N nanocomposite films, *J. Magn. Magn. Mater.* 321 (2009) 3149.

[24] L. Neél, Anisotropie magnétique superficielle et surstructures d'orientation, *J. Phys. Radium* 15 225 (1954).

[25] K. Seemann, S. Beirle, H. Leiste, On the in-plane uniaxial anisotropy formation by using Fe–Co–Zr–N films: a theoretical and experimental investigation, *J. Magn. Magn. Mater.* 413 (2016) 115.